CMS PAS SUS-13-025

DRAFT
CMS Physics Analysis Summary

2014/01/17
Head Id: 223486
Archive Id: 223616P
Archive Date: 2014/01/16
Archive Tag: trunk

Search for scalar top quark pair production in the dilepton final state at $\sqrt{s} = 8$ TeV with the CMS detector

The CMS Collaboration

Abstract

We report the results of a search for a scalar partner of the top quark (stop, $\tilde{t}$) using the full dataset of pp collisions at $\sqrt{s} = 8$ TeV collected by the CMS detector. We use a sample of opposite-sign dilepton events ($ee, \mu\mu, e\mu$) with at least two jets including at least one b-tagged jet to perform the search. The "stransverse mass" (M_{T2}) of the dilepton system with respect to the missing transverse energy is used to separate the stop signal from the dominant $t\bar{t}$ background. We see no excess of events above the standard model background. The results are interpreted in terms of several simplified models (SMS) which represent possible decays of the stop in R-parity conserving "natural" supersymmetric models where the stop is not the lightest supersymmetric particle.

1 Introduction

Supersymmetry (SUSY) is an extension of the Standard Model (SM) which provides a solution to the heirarchy problem by explaining why the Higgs mass can be near the electroweak scale without excessive fine tuning. In models where R-parity is conserved, the lightest supersymmetric particle (LSP) can also provide a candidate for the dark matter observed by astrophysicists. Early LHC data has provided strict limits on the production of generic colored superpartners using final states consisting of jets and missing energy. However, SUSY can still be natural if the superparters of the Higgs, top, and gluon have masses near the electroweak scale. Generic searches may not provide the best limits on these scenarios, so it is necessary to devise new search strategies targeted specifically to the natural scenarios.

This note presents results of a search for scalar top partners produced in pp collisions at a center-of-mass energy of $\sqrt{s} = 8$ TeV. We use events with two opposite-sign high-p_{T} isolated leptons, and at least two jets with at least one b-tagged jet to perform the search. The stransverse mass variable M_{T2} [1] is used to separate the stop signal from the Standard Model background, which consists primarily of $t\bar{t}$ production:

$$M_{T2}^2 = \min_{\mathbf{p}_{T1}^{miss} + \mathbf{p}_{T2}^{miss} = \mathbf{p}_T^{miss}} \left(\max \left[m_T^2(\mathbf{p}_T^{\ell 1}, \mathbf{p}_{T1}^{miss}), m_T^2(\mathbf{p}_T^{\ell 2}, \mathbf{p}_{T2}^{miss}) \right] \right) \tag{1}$$

It can be shown [1] that this definition of M_{T2} has the same convenient property as the transverse mass: it must be less than the mass of the pair-produced semi-invisbly decaying particle.

In the case of stop searches in the dilepton channel, the primary challenge comes from separating SM $t\bar{t}$ production from the signal, since the composition of the final states is identical except for invisible particles. Assuming that the contribution of the other products X to the $E_{\mathrm{T}}^{\mathrm{miss}}$ is not large, the assumptions made in the definition of M_{T2} hold for the lepton-$E_{\mathrm{T}}^{\mathrm{miss}}$ system and its value has an upper bound at the W mass. On the other hand, stop pair production events with a dileptonic final state will have at least four invisible particles so long as lepton number and R-parity are both conserved. Now there are two invisible particles on each side of the decay, and so the partition of the $E_{\mathrm{T}}^{\mathrm{miss}}$ into two components no longer has an upper bound at the W mass.

The analysis strategy described in the note uses this property of M_{T2} to define a signal region, $M_{T2} > M_W$, which should have a reduced contamination from dileptonic top decays. We estimate the residual contamination of the signal region with SM $t\bar{t}$ and WW events by normalizing simulated backgrounds in a data-driven way using several different control regions. Finally, we perform a counting experiment in the signal region and interpret the results in terms of several different simplified models (SMS) relevant for third generation or natural supersymmetry.

2 Selection

2.1 The CMS detector

The central feature of the CMS apparatus is a superconducting solenoid, 13 m in length and 6 m in diameter, which provides an axial magnetic field of 3.8 T. Within the field volume are several particle detection systems. Charged particle trajectories are measured with silicon pixel and strip trackers, covering $0 \leq \phi < 2\pi$ in azimuth and $|\eta| < 2.5$ in pseudorapidity, where $\eta = -\ln[\tan(\theta/2)]$ and θ is the polar angle of the trajectory of the particle with respect to the counterclockwise proton beam direction. A lead tungstate crystal electromagnetic calorimeter and a brass/scintillator hadron calorimeter surround the tracking volume, providing energy measurements of electrons and hadronic jets. Muons are identified and measured in gas-ionization detectors embedded in the steel flux return yoke of the solenoid. The CMS detector is nearly hermetic, allowing momentum balance measurements in the plane transverse to the beam direction. A two-tier trigger system selects pp collision events of interest for use in physics analyses. A more detailed description of the CMS detector can be found elsewhere [2].

2.2 Simulated samples

Monte Carlo (MC) simulations of signal and background processes are used to estimate the signal acceptance and provide information on the backgrounds that cannot be extracted directly from the data. Event samples for SM processes are generated using the PYTHIA 6.4.22 [3], MADGRAPH 5.1.3.30 [4], MC@NLO [5, 6], or POWHEG [7] MC event generators and the CTEQ6.6 parton density functions [8]. The most important background to the analysis is from SM $t\bar{t}$ events for which we use POWHEG for the “reference” $t\bar{t}$ sample. The MADGRAPH and MC@NLO generators are used for cross-checks and validations. All SM processes are normalized to cross section calculations at next-to-next-to-leading order (NNLO) when available, otherwise at next-to-leading order (NLO) [5, 6, 9–14].

For the signal events, the production of top-squark pairs is generated with MADGRAPH, including up to two additional partons at the matrix-element level. The decays of the top squarks are generated with PYTHIA. A grid of signal events is generated as a function of the top squark and neutralino masses with 25 GeV spacings.

In the MC samples, for both signal and backgrounds, multiple proton-proton interactions in the same or nearby bunch crossings (pileup) are simulated using PYTHIA and superimposed on the hard collision. The simulation of new physics signals is performed using the CMS fast simulation package [15], whereas almost all SM samples are simulated using a GEANT4-based model [16] of the CMS detector. The exceptions are the MADGRAPH $t\bar{t}$ samples used to study the sensitivity of estimated backgrounds to the details of the generator settings; these samples are processed with the fast simulation. The simulated events are finally reconstructed and analyzed with the same software used to process collision data.

2.3 Object selection

This analysis uses approximatley 20 fb^{-1} of 8 TeV collision data collected with dilepton triggers. Events came from one of three triggers: a dielectron trigger requiring two loosely isolated candidates with p_T greater than 17 and 8 GeV, a dimuon trigger requiring two muon candidates with p_T greater than 17 and 8 GeV, or a muon-electron trigger requiring one muon candidate and one loosely isolated electron candidate with p_T greater and 17 and 8 GeV in either permutation.

Electron candidates are required to have at least 20 GeV (10 GeV) of transverse momentum for the leading (lagging) candidate and fall within $-2.5 < \eta < 2.5$. We apply a standard veto on conversion electrons. Electron candidates are required to be isolated and to be consistent with the highest-p_T collision vertex in the event. Muon candidates are required to have at least 20 GeV (10 GeV) of transverse momentum for the leading (lagging) candidate and fall within $-2.4 < \eta < 2.4$. We require the transverse (longitudinal) impact parameter with respect to the primary vertex to be less than 2 (5) mm. Muons must also have high track quality and be isolated. Anti-k_t jets with distance parameter 0.5 are used, built from the particle flow algorithm [17] [18]. Jet candidates are required to have at least 30 GeV of transverse momentum and fall within $-2.4 < \eta < 2.4$. Jet are required to pass a loose jet identification, which selects

Object	Selection
e, μ	At least two, oppositely charged
	Highest sum-p_T pair used
M_{ee} or $M_{\mu\mu}$	$M < 76 \cup M > 106$
E_T^{miss}	> 40 in $ee, \mu\mu$ channels
$M_{\ell\ell}$	> 20 GeV (all flavors)
N_{jets}	≥ 2
N_b	≥ 1

Table 1: Event selection

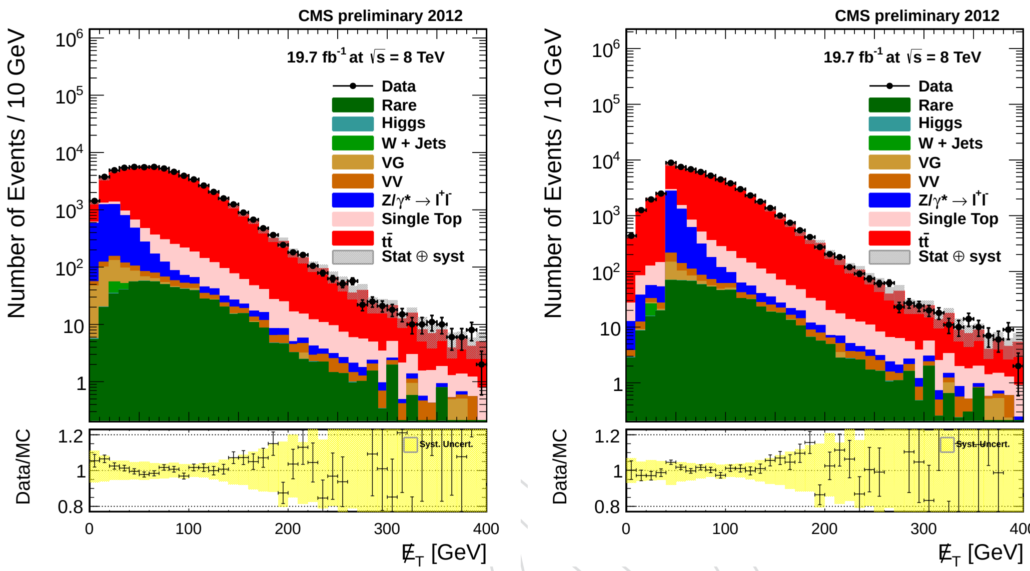

Figure 1: Selected events before (left) and after (right) the E_T^{miss} cut on same flavor events. The Drell-Yan contribution is efficiently removed by the E_T^{miss} requirement.

only jets with EM and hadronic energy fractions consistent with a real jet. In order to consider a jet as b-tagged we also require that the jet pass the medium working point of the combined secondary vertex (CSV) tagging algorithm [19].

2.4 Event selection

Using the object definitions from Section 2.3, we proceed to define an event selection shown in Table 1. We require at least two oppositely charged e and/or μ with an invariant mass larger that 20 GeV. Same-flavor lepton pairs are vetoed if the invariant mass of the leptons is within 25 GeV of the Z mass. In the case where both leptons have the same flavor (SF), we additionally ask for at least 40 GeV of E_T^{miss} in order to suppress the SM background from Drell-Yan pairs which pass the invariant mass requirement. We use the E_T^{miss} computed by the particle flow algorithm with a standard suite of corrections applied [18]. The effect of this requirement can be seen in Figure 1. To further suppress this and other vector boson backgrounds, we require at least two jets and one of them must be b-tagged.

2.5 Pile-up reweighting

The number of pile-up interactions per event affects the analysis in several ways. Pile-up reduces the probability of identifying the correct primary vertex in the event. It worsens the energy resolution for the selected objects (especially jets and E_T^{miss}), and makes lepton identification more difficult by putting additional energy into the isolation cones of lepton candidates.

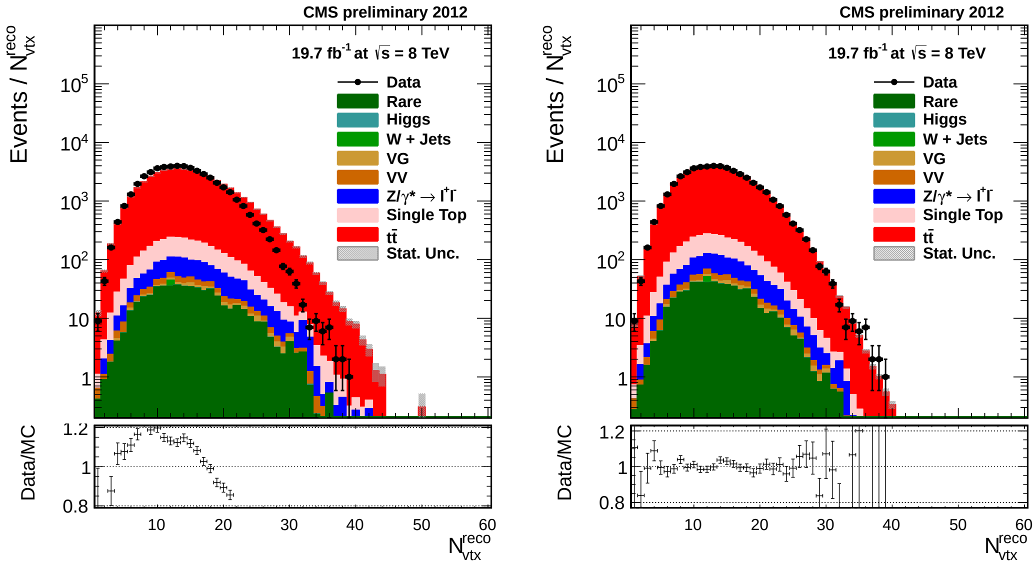

Figure 2: Number of reconstructed vertices in simulation and data, before reweighting (left) and after (right). Statistical uncertainty on simulation is indicated by the gray shaded band; on data, by black error bars. NB that signal and background Monte Carlo require different reweighting schemes.

It has similar effects at the trigger level. For all these reasons, we reweight the simulation events to have the same pile-up distribution as in data. Since the LHC ran at 50 ns bunch spacing in 2012, we are primarily concerned with the effect of in-time pileup. As a result, we determine the event weights using the Poisson mean for the true number of pileup vertices in the event. Figure 2 displays the number of reconstructed primary vertices in data and simulation, before and after the pile-up weights are applied. We apply the full object and event selection for this plot. The reweighting procedure results in good agreement between the distribution of number of vertices in the simulation with our selected data sample.

3 Backgrounds

The object selection described in Section 2 rejects most standard model backgrounds; only final states which contain two high-p_T lepton candidates along with two jets with one b-tag contribute to the background. The dominant sources of background and their approximate contributions to the selected sample for $M_{T2} > 80$ GeV are the following:

- $t\bar{t}$: 90%
- Drell-Yan: 4%
- tW: 4%
- diboson: <1%
- other (fake leptons): 1%

We evaluate the contributions of the Drell-Yan and fake lepton backgrounds in a data-driven way using control samples. The rate of the EW backgrounds is taken from simulation. The remainder is considered as $t\bar{t}$ and normalized to the control region with $MT_2 < 80$ GeV.

3.1 Description of the "$R_{out/in}$ method"

The analysis makes use of a data-driven Drell-Yan estimation method. We extract the so-called $R_{out/in}$ parameter, that is defined as the ratio of the events outside the Z-veto, as defined in 2.3, divided by the events falling inside that region:

$$R_{out/in} = \frac{N^{out}_{DYMC}}{N^{in}_{DYMC}} \tag{2}$$

This ratio is then applied to the number of data events falling inside the Z-veto region ($N^{l^+l^-}_{in}$) to predict the number of expected events in data ouside the Z-veto region. $N^{l^+l^-}_{in}$ can be contaminated by non-DY processes, such as $t\bar{t}$, therefore we subtract from $N^{l^+l^-}_{in}$ the number of events with opposite-flavour ($N^{e\mu}_{in}$). Since electrons and muons may have different reconstruction effieincies we use the k factors defined in Eq. 3 to account for these.

$$k_{ee} = \sqrt{\frac{N^{e^+e^-}_{in}}{N^{\mu^+\mu^-}_{in}}} \quad k_{\mu\mu} = \sqrt{\frac{N^{\mu^+\mu^-}_{in}}{N^{e^+e^-}_{in}}} \tag{3}$$

Hence the number of events outside the Z-veto window can be measured from data as:

$$N^{l^+l^-,obs}_{out} = R^{l^+l^-}_{out/in}(N^{l^+l^-}_{in} - 0.5N^{e\mu}_{in}k_{ll}) \tag{4}$$

where the factor 0.5 is used to account for combinatorics of the $e\mu$ sample.

3.1.1 Results using MC based $R_{out/in}$

The results obtained using this method are summarized in Tab. 2, the results are shown divided for the two same-flavor channels and for different stages of the selection. The differences between simulation and data driven estimates are coming from the discrepancies already observed in the $E_{\mathrm{T}}^{\mathrm{miss}}$ and jet distributions between data and MC.

3.1.2 Prediction in the opposite-flavor channel

The previous method can be simply applied in the $e\mu$ channel using the mean of the two scale factors, i.e. $SF_{e\mu} = \sqrt{SF_{ee} \times SF_{\mu\mu}}$, obtained for the ee and $\mu\mu$ channels.

3.2 Fake lepton estimation

Semileptonic top pair events and leptonically decaying W plus jets events can pass the signal selection if one of the jets in the event is misreconstructed as an isolated lepton. To guard against the possibility that the jet to lepton fake rate is not well modelled in the simulation, we perform a data-driven estimate of this probability using the so-called "tight-to-loose" method. As its name suggests, it relies on defining two working points for the muon and electron identification and isolation requirements: a tight one, which is the one used in the analysis, and a loose one, which defines the *"fakeable object"* and differs from the tight one because of relaxed

	≥ 2 jets	≥ 2 jets + $E_{\mathrm{T}}^{\mathrm{miss}}$	≥ 2 jets + $E_{\mathrm{T}}^{\mathrm{miss}}$ + b-tag
ee			
DY MC	14877.4 $\pm$ 53.0	2154.7 $\pm$ 18.0	236.13 $\pm$ 6.08
DY data-driven estimate	15613.0 $\pm$ 75.4	2626.2 $\pm$ 32.6	331.56 $\pm$ 14.54
$R_{out/in}$	0.1417 $\pm$ 0.0005	0.1644 $\pm$ 0.0015	0.1668 $\pm$ 0.0045
SF data/MC	1.0494 $\pm$ 0.0063	1.2188 $\pm$ 0.0183	1.4041 $\pm$ 0.0714
$\mu\mu$			
DY MC	27049.9 $\pm$ 73.6	4155.2 $\pm$ 25.2	415.00 $\pm$ 7.84
DY data-driven estimate	30217.7 $\pm$ 113.7	5361.6 $\pm$ 51.6	663.51 $\pm$ 22.68
$R_{out/in}$	0.1729 $\pm$ 0.0005	0.2144 $\pm$ 0.0014	0.2011 $\pm$ 0.0041
SF data/MC	1.1171 $\pm$ 0.0052	1.2904 $\pm$ 0.0147	1.5988 $\pm$ 0.0624
$e\mu$			
DY MC	2224.1 $\pm$ 16.5	-	208.65 $\pm$ 4.90
DY data-driven estimate	2408.0 $\pm$ 20.1	-	312.62 $\pm$ 12.42
SF data/MC	1.0827 $\pm$ 0.0041	-	1.4983 $\pm$ 0.0480

Table 2: Data-driven Drell-Yan background estimation in the ee and $\mu\mu$, and $e\mu$ channels compared with simulation, for several steps of the analysis. NB that no $E_{\mathrm{T}}^{\mathrm{miss}}$ cut is applied in the $e\mu$ case.

lepton isolation cuts. It consists of two steps. In the first one, fake and prompt rates are measured from data, in a phase space region enriched with QCD dijet events and $Z \to \ell\ell$ events, respectively. Both quantities are defined as the fraction of fakeable objects that also pass the tight selection. These ratios are parametrized as a function of p_T and η of the fakeable object.

In the second step, data events are required to pass the loose lepton requirements and the signal selection cuts. From this set of loose-loose dilepton events, the W+jets event yield can be extracted by means of some formulae combining fake and prompt rate.

The muon and electron prompt rates are obtained with a standard tag-and-probe technique applied on data.

The muon and electron fake rates are extracted from a phase space dominated by QCD dijet events. The cuts defining this control region aim at reducing the contribution from W or Z leptonic decays. Events with W decays are rejected by requiring PF $E_T^{miss} < 20$ GeV and, only for the muon fake rate, that the W candidate transverse mass be less than 15 GeV. Events with Z decays are discarded by vetoing the Z mass window: $m_{\mu\mu} \notin [76, 106]$ GeV, $m_{ee} \notin [60, 120]$ GeV. Events with low-mass dilepton resonances are removed by the additional $m_{\ell\ell} > 20$ GeV requirement.

The bias introduced by electroweak contaminations from leptons in W+jets and Z+jets events is removed in two ways. The tight (loose) lepton yields obtained from W+jets and Z+jets simulated samples are subtracted from data in the numerator (denominator) of the fake rate definition. Moreover, the residual bias for high p_T^{ℓ} values is avoided by assuming that lepton fake rate flattens out for $p_T^{\ell} > 35$ GeV.

An additional threshold is introduced on the p_T of a so-called *"away-side"* jet. It is a jet that is separated by at least $\Delta R(j_{away}, \ell) > 1.0$ from a loose lepton, which is required to be within a distance $\Delta R(j_{away}, \ell) < 0.3$ from a so-called *"near-side"* jet. This jet p_T requirement is motivated by the fact that the energy spectrum of jets misidentified as leptons can be different from the one of real jets. The relative isolation of a loose lepton is a sensitive variable to these differences in jet energy. Hence, by cutting on the away-side jet p_T (not on the near-side one, to avoid biases), the di-jet control sample from which the fake rate is extracted can be made more similar to the

after $N_{b-tags} \geq 1$				
channel	central value	stat.	syst.	stat. $\oplus$ syst.
$\mu\mu$	642	$\pm$18%	$\pm$4%	$\pm$18%
ee	97	$\pm$27%	$\pm$15%	$\pm$31%
$e\mu$	643	$\pm$28%	$\pm$6%	$\pm$29%
after $M_{T2}(\ell\ell) > 110$ GeV				
channel	central value	stat.	syst.	stat. $\oplus$ syst.
$\mu\mu$	1.09	$\pm$37%	$\pm$15%	$\pm$40%
ee	0.89	$\pm$24%	$\pm$18%	$\pm$30%
$e\mu$	0.91	$\pm$32%	$\pm$12%	$\pm$34%

Table 3: Estimated fake lepton events in the 1 b-tag sample and for one representative high-M_{T2} signal regions.

non-prompt background component contributing to the final event yield.

The lepton yields, extrapolated from the loose-loose to the tight-tight same-sign dilepton region, obtained with different requirements on the away-side jet p_T and on the loose lepton isolation, are compared with the ones extracted from data events containing a tight-tight same-sign lepton pair, with one lepton passing the quality criteria used in the analysis, the other one a looser selection. Contaminations from processes different from semileptonic or all-hadronic $t\bar{t}$ and from W+jets have been estimated from simulation and subtracted from this control sample. The threshold on jet p_T is then chosen as the one giving the best agreement. The results of this procedure give an η and p_{T} dependent fake rate for electrons and for muons.

To extract the non-W/Z lepton event yield, the event selection is applied to data, but requiring that both leptons pass the loose lepton quality cuts. Events are weighted by the number of leptons passing or failing the tight requirements. The total yield of fake lepton events is then given by the sum of event weights in the selected final state. Results are shown in Table 3 together with the statistical and systematical uncertainties.

3.3 $t\bar{t}$ estimation

After determining the contribution to the control region $M_{T2} < 80$ GeV from Z events and fake leptons by the previously described methods, and of the rare backgrounds from simulation, we estimate the normalization of the remaining top pair background by subtracting these estimates from the number of data events with $M_{T2} < 80$ GeV in both data and simulation and then scaling the number of $t\bar{t}$ events in the simulation to match the data. We obtain a scale factor of 1.007 with negligible statistical uncertainty. The normalization to the control region is displayed in Figure 3 for events passing the full object and event selection.

Signal contamination in the normalization region is handled using the Monte Carlo prediction. The fraction of signal misidentified as tt when performing this procedure is tracked for each signal point, and the overprediction of the background is accounted for in the limit-setting procedure. In general the effect is vanishingly small except at low mass when the splitting between the top and LSP mass is equal to the top mass, when the signal contamination can be as high as 10% and the shapes are similar for signal and background. Otherwise, the effect is typically of order one per mille.

One feature of Figure 3 which is not directly related to the background normalization yet bears some discussion is the peak in the M_{T2} distribution near zero. Since the computation of M_{T2} involves finding the minimum possible value for each event, solutions with $M_{T2} = 0$ will

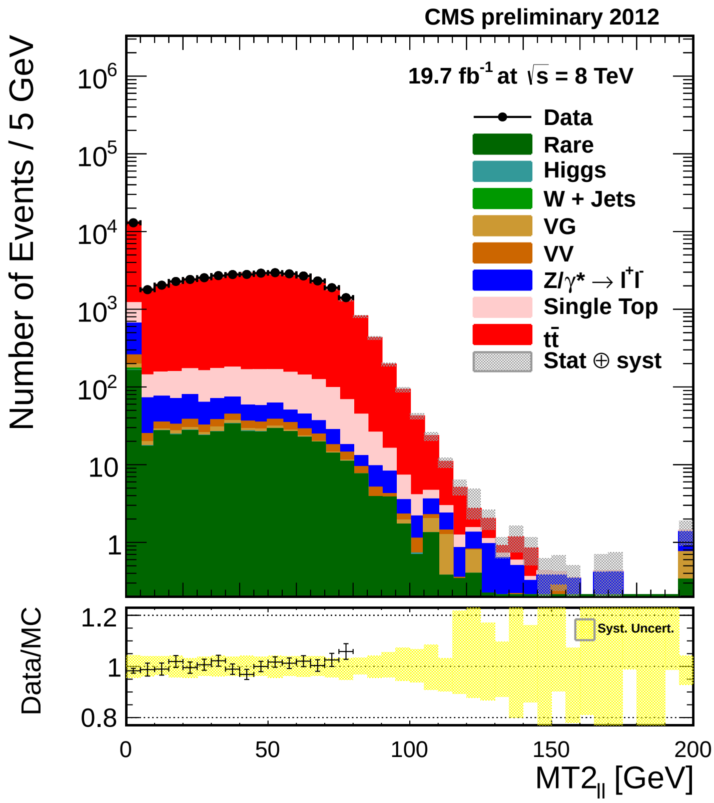

Figure 3: $M_{T2}(ll)$ distribution, used to obtain the normalization and normalization uncertainty for $t\bar{t}$ events.

Bkg.	Events	Stat. unc.	Sys. unc.
$t\bar{t}$	15.2	1.6	+4.3 -1.5
DY + jet(s)	5.9	0.8	+2.9 -1.5
$V\gamma$	1.8	0.8	+3.2 -0.9
single t	2.0	0.1	+0.2 -0.2
VV	0.6	0.2	+0.2 -0.3
other (e.g. W, H)	2.7	0.2	+0.6 -0.5

Table 4: Background prediction in the signal region $M_{T2} > 110$ GeV with statistical (MC statistics) and systematic uncertainties.

be kept if found. An example of an event for which $M_{T2} = 0$ would be one with back-to-back leptons, where the $E_{\mathrm{T}}^{\mathrm{miss}}$ vector points along one of the lepton vectors. In this case, any partition of the $E_{\mathrm{T}}^{\mathrm{miss}}$ vector along the lepton-lepton line will result in identically zero M_T for each side of the system and a total M_{T2} of zero. Other configurations can also have an M_{T2} of zero so long as a solution with zero transverse mass along each lepton can be found.

3.4 Summary

Estimated background yields and their associated uncertainties for $M_{T2} > 110$ GeV are displayed in Table 4. The mean background expectation for five different M_{T2} cuts are displayed in Table 5.

M_{T2} value	Expected bkg.	Stat. unc.	Sys. unc.	
80	1702.4	17.2	+110.6	-113.1
90	414.0	8.2	+44.0	-38.8
100	101.5	3.9	+11.5	-12.7
110	28.2	2.0	+7.1	-2.4
120	12.9	1.2	+3.4	-1.4

Table 5: Background expectation for five different M_{T2} cut values.

Source	Uncertainty
ϵ(trigger)	1.2%
$\epsilon(\ell)$	1.8%
ℓ energy scale	1.7%
ϵ(b-tag)	5.0%
gen top p_{T}	0.5%
JES	13.5%
JER	9.3%
unclustered energy	7.3%
Total	19.1%

Table 6: Systematic uncertainties on the background yield in the signal region $M_{T2} > 110$ GeV by source. In cases where the error is asymmetric the larger of the two errors is displayed. The full asymmetric error is used in the limit calculation.

4 Systematic uncertainties

The sensitivity of this analysis is affected both by uncertainties on the background contribution in the signal region as well as on the acceptance and efficiency for the signal models considered. Here we present studies of the size of the dominant systematic uncertainties.

4.1 Trigger efficiencies

The method uses events selected by a trigger selection weakly correlated with dilepton triggers (cross triggers) and counts the number of such events passing and failing the dilepton trigger selection. The MET based datasets were selected as the cross triggers, as they were found to be weakly correlated with dilepton triggers and to have a large enough number of events to keep the statistical uncertainty below 1%. The measured efficiencies were compared to the efficiencies in MC for $t\bar{t}$ events and the signal sample. In both cases the corresponding pileup corrections were applied. The principle of this method to estimate the inclusive trigger selection efficiency can be described as follow :

- Determine a set of triggers (cross triggers) weakly correlated with the dilepton triggers used in the analysis,
- Count the number of events N_{Xtrig} passing the cross triggers and the $t\bar{t}$ dilepton events selection,
- Count the number of events $N_{Xtrig+DILtrig}$ which pass the cross triggers selection, the $t\bar{t}$ dilepton events selection and the dilepton trigger selection.

The resulting p_{T}- and η-dependent scale factors and uncertainties are propagated to the final yields. The scale factors range from 0.94 to 1.00 depending on the p_{T} and η considered, with uncertainties in the range of 0.01–0.03.

4.2 Lepton identification and isolation efficiencies

Lepton efficiencies are estimated using a tag and probe method, following a simple cut and count based approach (except for the lowest p_{T} bin, where a fit is used to account for the non negligible background contribution). In order to estimate the efficiency such that the measurement is uncorrelated from the dilepton trigger efficiency, single lepton triggered data samples are used. Dilepton candidates compatible with the Z mass are assumed to come from the Z bosons and used to estimate the efficiency. The tag and probe leptons are matched requiring opposite charge and an invariant mass in the range $76 < \mathrm{m}_{ll} < 106$ GeV. The definition of "tag" leptons corresponds to the complete isolation and identification used in the analysis. Tag leptons in both channels are selected if they are associated to an HLT lepton. The measured efficiencies are compared to the results in MC Drell-Yan (FullSim and FastSim), where the pileup correction is applied to extract the scale factors ($SF_l = \epsilon_l^{data}/\epsilon_l^{MC}$) used to correct the MC predictions. The global identification and isolation efficiencies and scale factors are presented in Table **??**, both for the full and fast simulation samples.

	Eff Data	Eff. FullSim	SF FullSim	Eff. FastSim	SF FastSim
Muon	0.9361±0.0001	0.9452±0.0001	0.9904±0.0002	0.9715±0.0001	0.9636±0.0002
Electron	0.7871±0.0002	0.8114±0.0002	0.9701±0.0002	0.8452±0.0002	0.9312±0.0002

Table 7: Muon and electron identification and isolation efficiencies, measured in data and with the Drell-Yan samples (full and fast simulation). The errors correspond only to the statistical uncertainty.

The systematic uncertainties of the lepton efficiencies are estimated by varying the invariant mass window and the tag lepton selection and reapplying the tag and probe method. The largest variation of the scale factors with respect to their nominal value found is about 0.5%. A total systematic uncertainty of 1% in the scale factor is considered, to account as well for differences between Z and $t\bar{t}$-like event kinematics. The resulting scale factors and uncertainties are propagated through to the final yields.

We do not observe any substantial correlation between the value of M_{T2} and the size of the systematic uncertainty.

4.3 *b*-tag efficiency

We use the *b*-tag efficiency scale factors and associated uncertainties obtained from comparison of *b*-enriched control samples in data with the simulated preformance.. We then vary the scale factor in simulation between $\pm 1\sigma$ from the central value and track the change in the expected background yield in the signal region. NB that separate factors are used for FullSim and FastSim samples.

4.4 Jet Resolution Correction for the measurement of $E_{\mathrm{T}}^{\mathrm{miss}}$

The simulation doesn't model the energy resolution of jets with full accuracy. This subsequently affects the modeling of $E_{\mathrm{T}}^{\mathrm{miss}}$ in the simulation. We use a tool that smears the energy of jets in the simulation propagates these smeared jets into the $E_{\mathrm{T}}^{\mathrm{miss}}$. Utilizing a separate set of simulation samples with representative event topologies – $t\bar{t}$, DY + jets, etc. – we calculated the effects of this smearing on the two components of the $E_{\mathrm{T}}^{\mathrm{miss}}$ vector and the dependence of this smearing on the event's unsmeared $E_{\mathrm{T}}^{\mathrm{miss}}$. We then utilized these calculated results as template smearing functions to generate smeared $E_{\mathrm{T}}^{\mathrm{miss}}$ vectors for the $E_{\mathrm{T}}^{\mathrm{miss}}$ in our simulation samples.

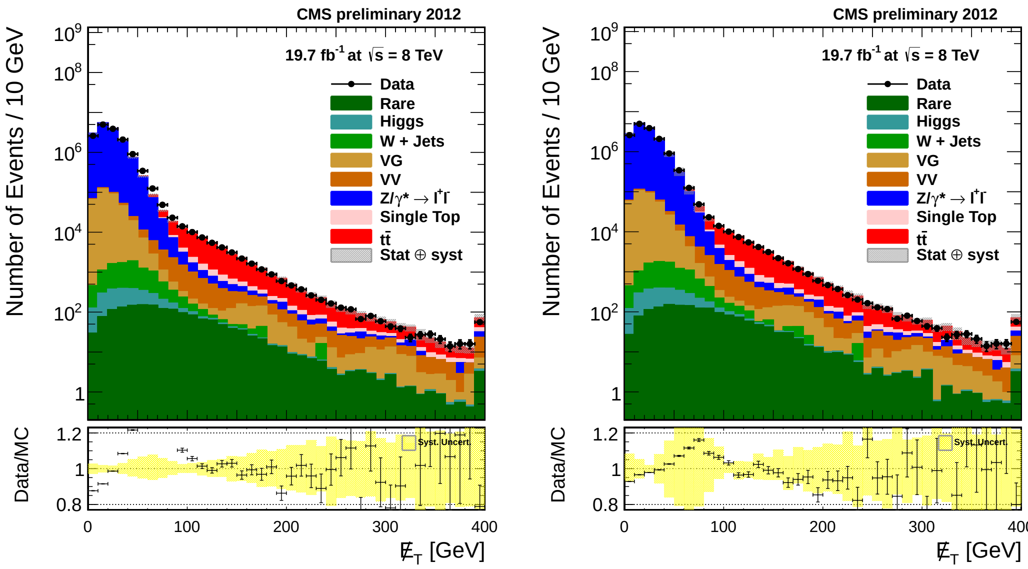

Figure 4: $E_{\mathrm{T}}^{\mathrm{miss}}$ distribution in the inclusive dilepton sample before (left) and after (right) correcting the JER in simulation. Note that the modeling of the DY + jets background below 100 GeV is much better post-smearing.

Due to their small contribution in the signal region we did not apply this process to the rare backgrounds.

The results of this smearing are shown in Figure 4.

4.5 $E_{\mathrm{T}}^{\mathrm{miss}}$ uncertainties propagated to M_{T2}

The $E_{\mathrm{T}}^{\mathrm{miss}}$ measurement is affected by uncertainties on the energy scales and resolutions of all other objects in the event. Of special concern are the uncertainties on jet energy scale, jet energy resolution, and the scale of the unclustered energy in the event. In order to evaluate the effect of these uncertainties we utilized a combination of several prescriptions.

For the lepton and jet energy scales, we varied the objects within systematic uncertainties taken from their respective POGs, propagating the shifted objects back into the $E_{\mathrm{T}}^{\mathrm{miss}}$ calculation. For the leptons, the shifted objects themselves are also used in the calculation of M_{T2}.

For the unclustered energy scale and jet energy resolution uncertainties we utilized the separate simulation samples mentioned in Section 4.4. In addition to the information on smeared $E_{\mathrm{T}}^{\mathrm{miss}}$, these samples also contain separate versions of the smeared $E_{\mathrm{T}}^{\mathrm{miss}}$ where the smearing factors (i.e. magnitude of the smearing) for the jets have been varied within $\pm 1\sigma$ of the central value and where the energy scale for unclustered PF candidates has been varied within $\pm 1\sigma$ (10%) of the central value. As with the basic smearing, we calculated template smearing functions with the systematic shifted versions (unclustered energy scale and JER smearing factor) of $E_{\mathrm{T}}^{\mathrm{miss}}$. We propagated all calculated systematic uncertainties on the $E_{\mathrm{T}}^{\mathrm{miss}}$ measurement to the M_{T2} measurement by recalculating M_{T2} for each systematic shift version of the $E_{\mathrm{T}}^{\mathrm{miss}}$ measurement.

4.6 Other systematics

Since the rare electroweak background yields are estimated from simulation, we varied the normalization of these backgrounds in order to check the effects in case the true cross section is far from the prediction. Even with an extreme variation of 50% of the cross section the change in the background yield was at the one percent level since these backgrounds make up only a

M_{T2} value	Data	Expected bkg.	Stat. unc.	Sys. unc.	
80	1784	1702.4	17.2	+110.6	-113.1
90	426	414.0	8.2	+44.0	-38.8
100	106	101.5	3.9	+11.5	-12.7
110	30	28.2	2.0	+7.1	-2.4
120	14	12.9	1.2	+3.4	-1.4

Table 8: Data yields and background expectation for five different M_{T2} cut values.

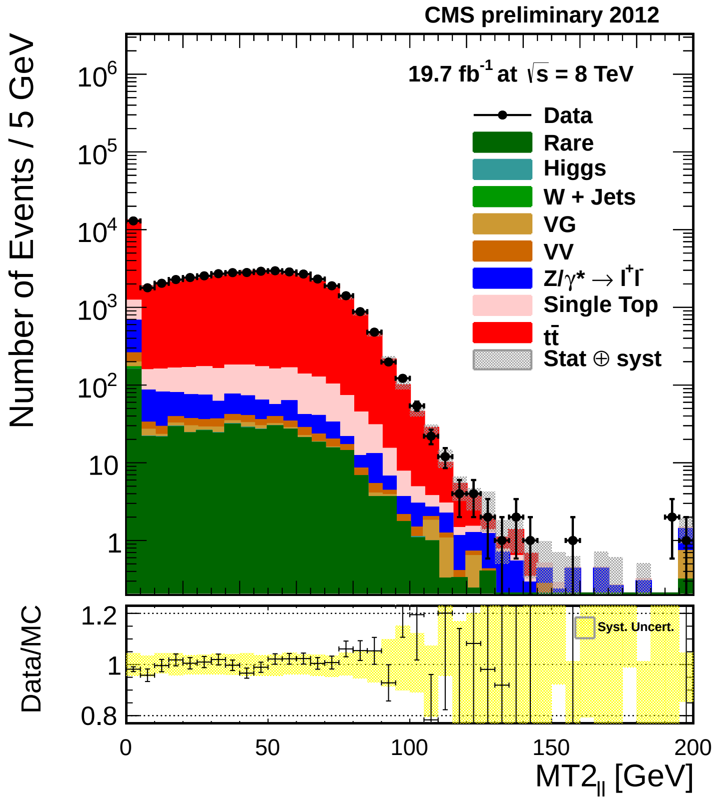

Figure 5: Full unblinded M_{T2} distribution with full systematics.

few percent of the total yield. Since the other uncertainties are much larger we do not use this uncertainty in the final result.

We also considered the effect of variations of the W mass on the background yield. However the current world average uncertainty on the W mass is only 15 MeV and the uncertainty on the width is only 42 MeV. Since these uncertainties are much smaller than the $E_{\mathrm{T}}^{\mathrm{miss}}$ resolution and therefore much smaller than the M_{T2} resolution we do not use this uncertainty in the final result.

The composite effect of all systematic uncertainties is shown in Figure 3.

5 Results

Table 8 shows the background predictions of Table 5 along with the observed number of events in the unblinded signal region in data.

Figure 5 shows the full unblinded M_{T2} distribution. Figures 6 and 7 show the same distribution with example signal models for $M_{stop} = 300$ GeV. The agreement between data and the

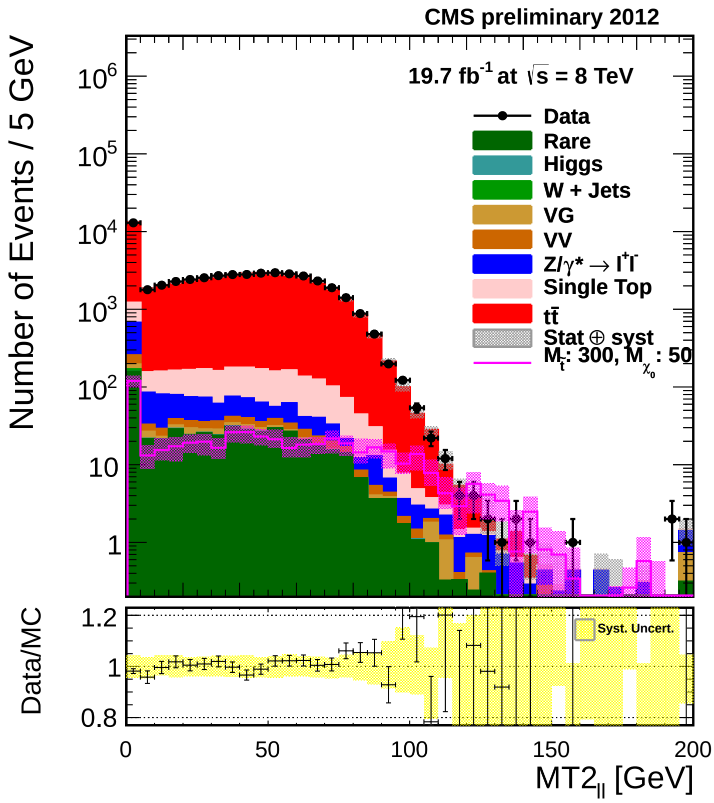

Figure 6: Full unblinded M_{T2} distribution with full systematics. For comparison, a T2tt model point with 300 GeV stop and 50 GeV LSP is shown in magenta.

backgound prediction in the signal region is excellent in all cases. Since we observe no excess over the SM background we proceed to set limits.

6 Limit setting

The theoretical prediction for the stop cross section used for the limit calculation is shown in Figure 8. The same cross section for stop production is used regardless of the decay mode considered.

The acceptance for each point is derived from the simulation as shown in Figure 9. For each point, we use the cut on M_{T2} which gives the best expected limit on the signal strength given the yields in simulation. Cut values between 80 and 140 GeV were tested in steps on 10 GeV, but for T2tt, cuts above 120 GeV never give the best limit due to very small signal efficiency. Lower cuts (80 to 90 GeV) give some sensitivity in the region where the top decay is off-shell, as shown in Figure 10. The same procedure for establishing the systematic uncertainty in the background yield is used at each signal point to derive a systematic uncertainty on the signal acceptance at that point. In addition to the uncertainties on background we include an additional term for the uncertainty in the stop cross section at NLO as computed by the LPCC SUSY cross section working group.

Expected limits for the T2tt SMS in the (stop mass, neutralino mass) plane are shown in Figure 11. (NB that these limits are computed with the asymptotic setting of the Higgs Combine tool for now, we will do the full computation once things are more stable.)

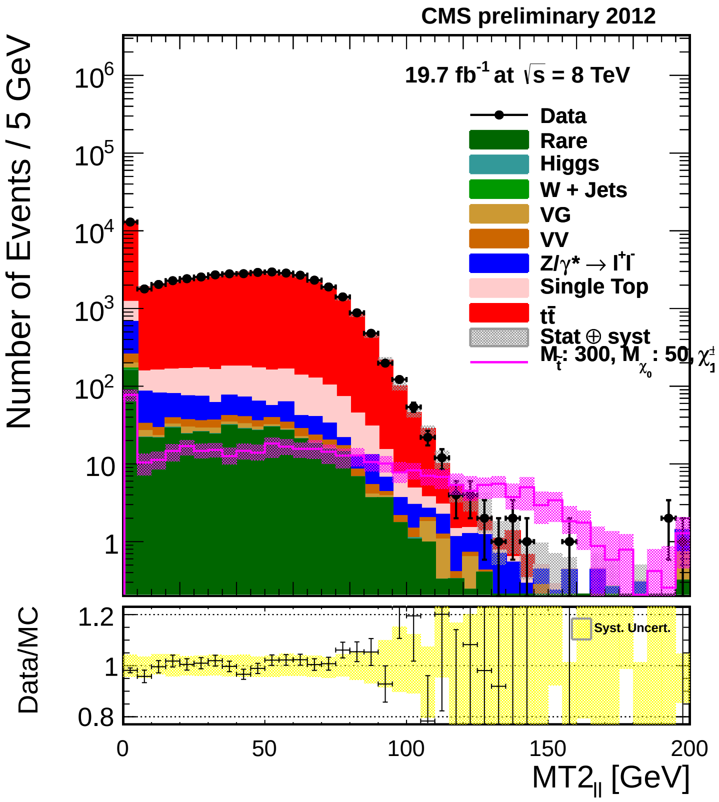

Figure 7: Full unblinded M_{T2} distribution with full systematics. For comparison, a T2bw model point with 300 GeV stop, 50 GeV LSP, and 190 GeV chargino is shown in magenta.

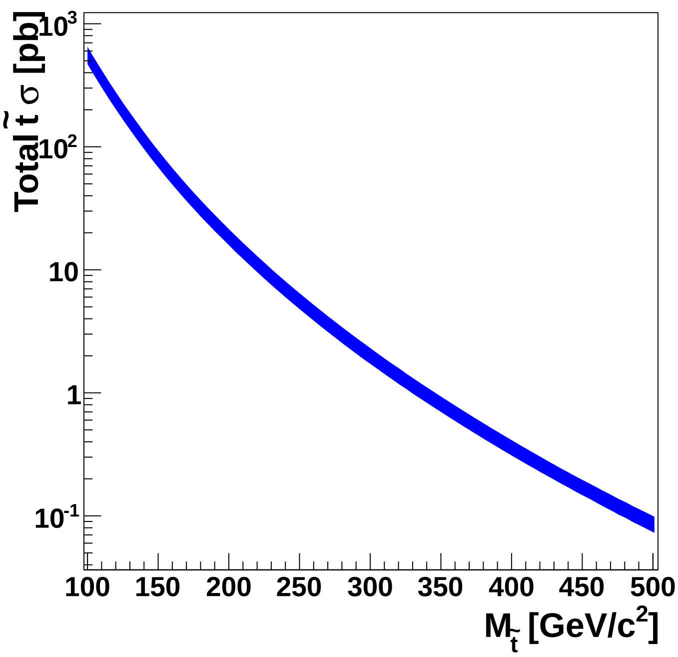

Figure 8: Stop cross section as a function of mass as used in the limit setting. The blue band indicates the systematic uncertainty on the stop cross section.

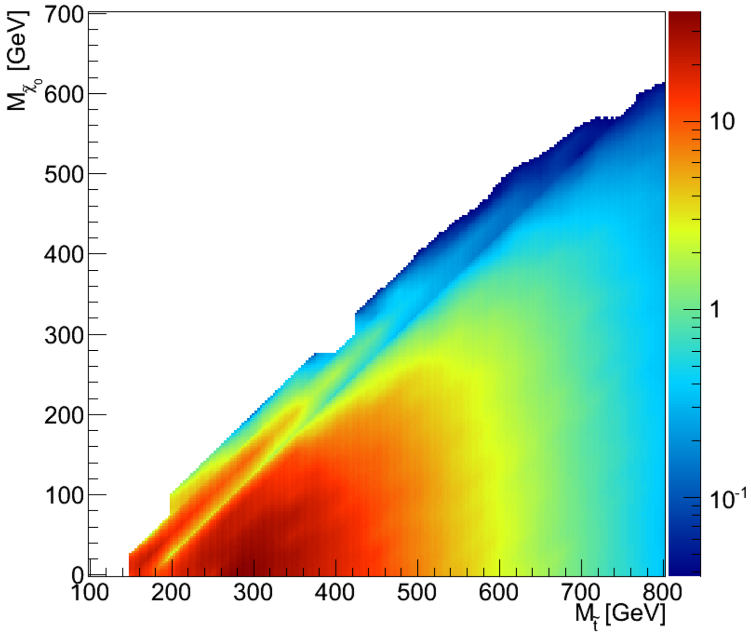

Figure 9: Signal yield of the selection for the T2tt SMS with a cut of 110 GeV on M_{T2} for the integrated luminosity used in this analysis. The diagonal feature that intersects the x-axis at the top mass corresponds to model points for which the mass splitting between the stop and χ^0 is equal to the top mass. Points above the line therefore have off-shell top decays.

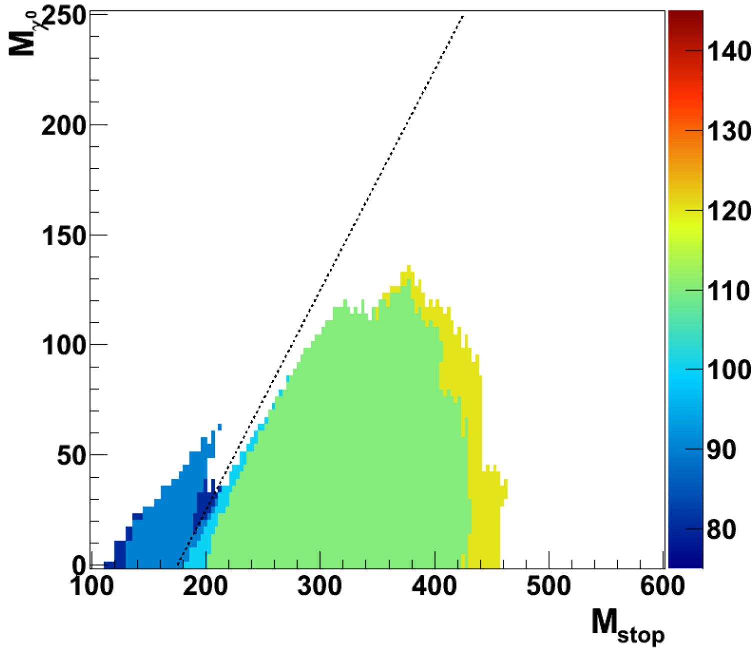

Figure 10: Output of the optimiztion of M_{T2} cut for the T2tt signal model. The dotted line indicates the model points for which the mass splitting between the stop and χ^0 is equal to the top mass. The z-axis shows which cut value gives the best expected limit on the signal strength. Points inaccessible for this analysis strategy are left uncolored.

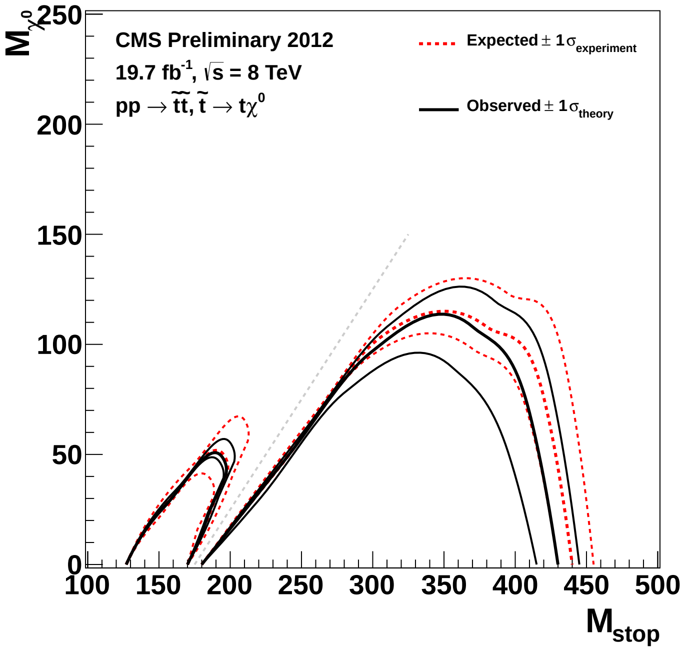

Figure 11: 95% CL expected limits for the T2tt SMS in the stop mass, neutralino mass plane.

References

[1] C. G. Lester and D. J. Summers, "Measuring masses of semiinvisibly decaying particles pair produced at hadron colliders", *Phys. Lett.* **B463** (1999) 99–103, `doi:10.1016/S0370-2693(99)00945-4`, `arXiv:hep-ph/9906349`.

[2] CMS Collaboration, "The CMS experiment at the CERN LHC", *J. Inst* **3** (2008) S08004, `doi:10.1088/1748-0221/3/08/S08004`.

[3] T. Sjöstrand, S. Mrenna, and P. Z. Skands, "PYTHIA 6.4 Physics and Manual", *JHEP* **05** (2006) 026, `doi:10.1088/1126-6708/2006/05/026`, `arXiv:hep-ph/0603175`.

[4] J. Alwall et al., "MadGraph 5 : Going Beyond", *JHEP* **1106** (2011) 128, `doi:10.1007/JHEP06(2011)128`, `arXiv:1106.0522`.

[5] S. Frixione and B. R. Webber, "Matching NLO QCD computations and parton shower simulations", *JHEP* **0206** (2002) 029, `arXiv:hep-ph/0204244`.

[6] S. Frixione, P. Nason, and B. R. Webber, "Matching NLO QCD and parton showers in heavy flavor production", *JHEP* **0308** (2003) 007, `arXiv:hep-ph/0305252`.

[7] S. Frixione, P. Nason, and C. Oleari, "Matching NLO QCD computations with parton shower simulations: the POWHEG method", *JHEP* **11** (2007) 070, `doi:10.1088/1126-6708/2007/11/070`, `arXiv:0709.2092`.

[8] P. M. Nadolsky et al., "Implications of CTEQ global analysis for collider observables", *Phys. Rev. D* **78** (2008) 013004, `doi:10.1103/PhysRevD.78.013004`, `arXiv:0802.0007`.

[9] N. Kidonakis, "Differential and total cross sections for top pair and single top production", `doi:10.3204/DESY-PROC-2012-02/251`, `arXiv:1205.3453`.

[10] J. M. Campbell and R. K. Ellis, "$t\bar{t}W^{+-}$ production and decay at NLO", *JHEP* **1207** (2012) 052, doi:10.1007/JHEP07(2012)052, arXiv:1204.5678.

[11] M. Garzelli, A. Kardos, C. Papadopoulos, and Z. Trocsanyi, "t $\bar{t}$ W^{+-} and t $\bar{t}$ Z Hadroproduction at NLO accuracy in QCD with Parton Shower and Hadronization effects", *JHEP* **1211** (2012) 056, doi:10.1007/JHEP11(2012)056, arXiv:1208.2665.

[12] J. M. Campbell and R. Ellis, "MCFM for the Tevatron and the LHC", *Nucl.Phys.Proc.Suppl.* **205-206** (2010) 10–15, doi:10.1016/j.nuclphysbps.2010.08.011, arXiv:1007.3492.

[13] R. Gavin, Y. Li, F. Petriello, and S. Quackenbush, "W Physics at the LHC with FEWZ 2.1", *Comput.Phys.Commun.* **184** (2013) 208–214, doi:10.1016/j.cpc.2012.09.005, arXiv:1201.5896.

[14] R. Frederix et al., "Four-lepton production at hadron colliders: aMC@NLO predictions with theoretical uncertainties", *JHEP* **1202** (2012) 099, doi:10.1007/JHEP02(2012)099, arXiv:1110.4738.

[15] CMS Collaboration, "The fast simulation of the CMS detector at LHC", *J. Phys. Conf. Ser.* **331** (2011) 032049, doi:10.1088/1742-6596/331/3/032049.

[16] GEANT4 Collaboration, "GEANT4–a simulation toolkit", *Nucl. Instrum. Meth. A* **506** (2003) 250, doi:10.1016/S0168-9002(03)01368-8.

[17] M. Cacciari, G. P. Salam, and G. Soyez, "The Anti-k(t) jet clustering algorithm", *JHEP* **0804** (2008) 063, doi:10.1088/1126-6708/2008/04/063, arXiv:0802.1189.

[18] CMS Collaboration, "Commissioning of the Particle-Flow Reconstruction in Minimum-Bias and Jet Events from pp Collisions at 7 TeV", CMS Physics Analysis Summary CMS-PAS-PFT-10-002, (2010).

[19] CMS Collaboration Collaboration, "Identification of b-quark jets with the CMS experiment", *JINST* **8** (2013) P04013, doi:10.1088/1748-0221/8/04/P04013, arXiv:1211.4462.

A Examination of data events with high M_{T2}

We chose three events in data with M_{T2} greater than 190 GeV to examine in detail, as a cross-check in case the large observed value was due to unexpected detector effects or reconstruction failures. NB that the number of high M_{T2} events is predicted with good accuracy by the simulation, so we expect to find mostly genuine physics events where well-understood detector acceptance or resolution effects have introduced spuriously high $E_{\mathrm{T}}^{\mathrm{miss}}$ values.

The first event is shown in Figure 12. The M_{T2} for this event is 190 GeV. It is a $\mu\mu$ event containing six jets above 50 GeV. The large value of M_{T2} comes from the $E_{\mathrm{T}}^{\mathrm{miss}}$ pointing opposite to the high p_{T} $\mu\mu$ system. The mass of the dilepton system is 43 GeV, the $E_{\mathrm{T}}^{\mathrm{miss}}$ is 140 GeV, and the angle between them is 2.7 radians. The $E_{\mathrm{T}}^{\mathrm{miss}}$ points near a high (180 GeV) p_{T} jet which is almost perfectly back-to-back with the dilepton system. One possible explanation for this event is that this recoiling jet is badly mismeasured. Close inspection of the objects in the event did not reveal any irregularities.

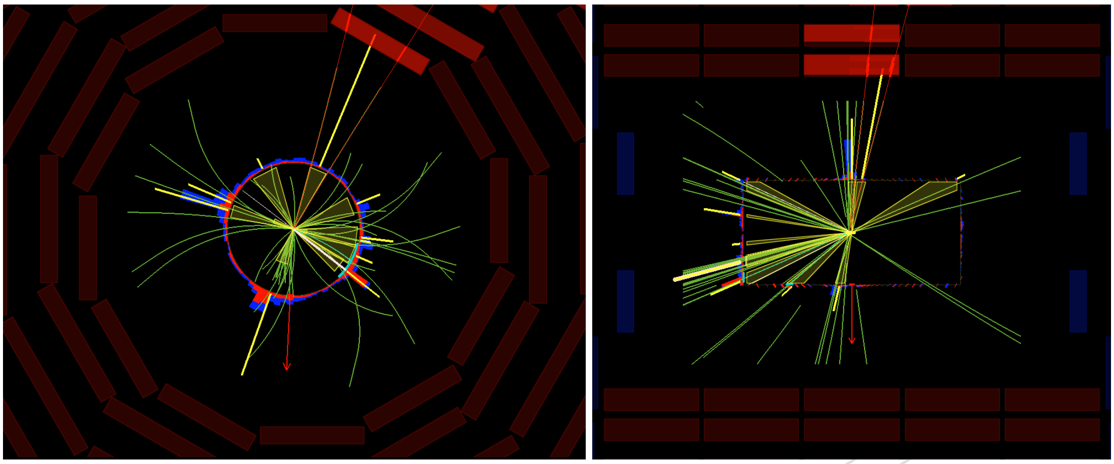

Figure 12: High-M_{T2} $\mu\mu$ event number 1.

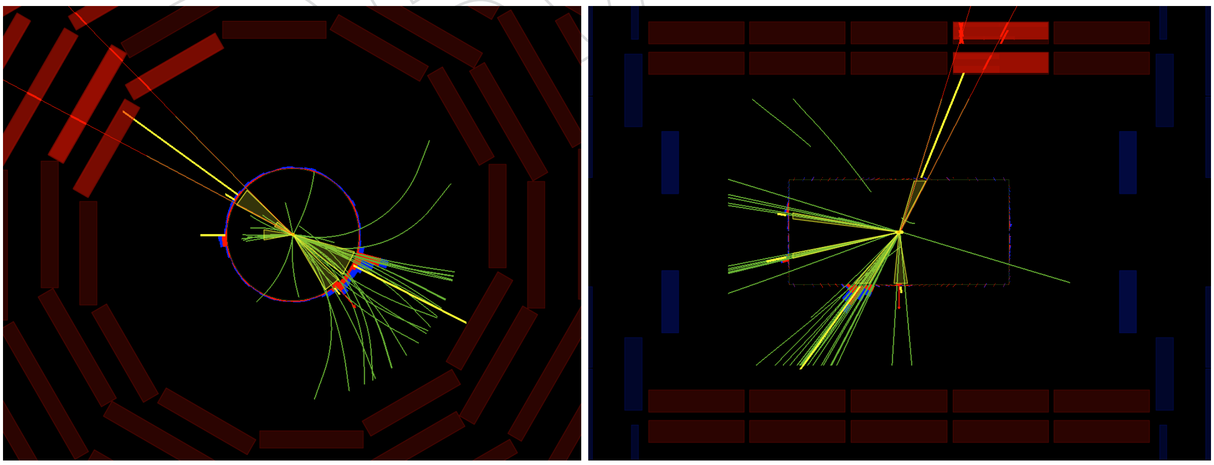

Figure 13: High-M_{T2} $\mu\mu$ event number 2.

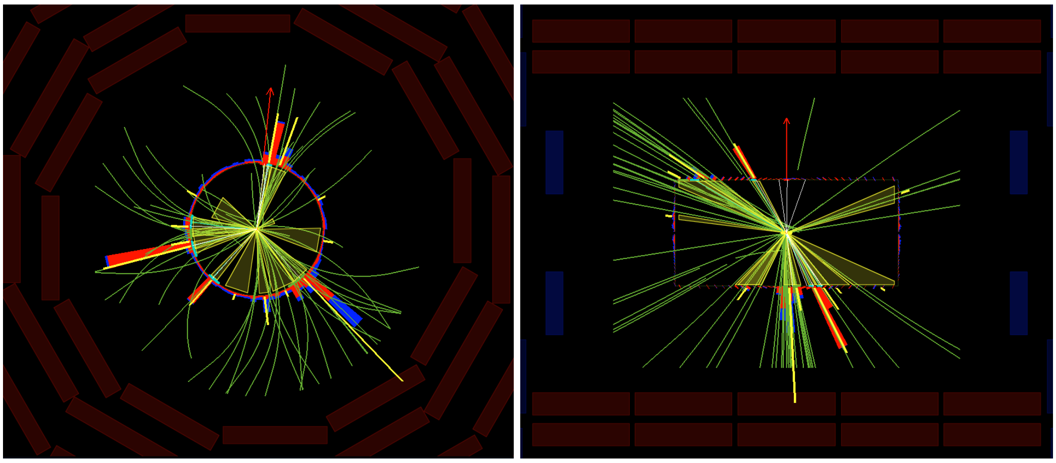

Figure 14: High-M_{T2} ee event number 3.

The second event is shown in Figure 13. The M_{T2} for this event is also 190 GeV. It is a $\mu\mu$ event with three jets above 50 GeV. Again, the $E_{\mathrm{T}}^{\mathrm{miss}}$ points opposite to the high p_{T} $\mu\mu$ system. The mass of the dilepton system is 75 GeV, falling just outside the Z veto window which starts at 76 GeV. The $E_{\mathrm{T}}^{\mathrm{miss}}$ is 100 GeV and the angle between the leptons and the $E_{\mathrm{T}}^{\mathrm{miss}}$ is 2.9 radians. Likely this is a $Z \to \mu\mu$ event where the hadronic recoil is mismeasured.

The third event is shown in Figure 14. It is an ee event, but the electrons (in cyan) are not easily seen due to the large multiplicity of high p_{T} particles in this event. The M_{T2} for this event is about 270 GeV, a remarkable value. The event had an extremely large amount of activity with seven jets above 50 GeV. The invariant mass of the electron pair is 106.3 GeV, falling just above the Z veto window which ends at 106 GeV. The $E_{\mathrm{T}}^{\mathrm{miss}}$ is aligned near two of the high p_{T} recoiling jets, so it is likely that this is a $Z \to ee$ event where the hadronic recoil is mismeasured.

NB that all three events are same-flavor as anticipated by the simulation, as high-multiplicity $Z + X$ events contribute to the tails much more in same-flavor channels.